

PAPER Nr. : 6



FIFTEENTH EUROPEAN ROTORCRAFT FORUM

SEPTEMBER 12 - 15, 1989 AMSTERDAM

FIFTEENTH EUROPEAN ROTORCRAFT FORUM

Paper No. 6

THE INFLUENCE OF INTERACTIONAL AERODYNAMICS
OF ROTOR-FUSELAGE-INTERFERENCES ON THE FUSELAGE FLOW

F.-W. MEYER

INSTITUTE FOR FLIGHTMECHANIC
TECHNISCHE UNIVERSITÄT BRAUNSCHWEIG
BRAUNSCHWEIG, GERMANY

September 12-15, 1989

AMSTERDAM, THE NETHERLANDS

THE INFLUENCE OF INTERACTIONAL AERODYNAMICS
OF ROTOR-FUSELAGE-INTERFERENCES ON THE FUSELAGE FLOW

F.-W. MEYER

Abstract

The paper presents a model which enables determination of aerodynamic data and boundary layer effects of the fuselage of an helicopter under the interactional aerodynamics of rotor-fuselage-interferences. The model is based on iterative calculation processes which are combined to a solution procedure. Although there are some complex methods such as panel and integral three-dimensional boundary layer and free wake-methods involved, the solution procedure needs only common computers. The modelling of the fuselage flow consists of a superposition of the influence of free stream velocity, fuselage angle of attack and rotor downwash. The rotor downwash is calculated by blade-element-theory and momentum considerations, the wake is represented by a time-averaged free wake model. The model provides insight to the problem and improves the understanding of the "secondary" effects of interactional aerodynamics of rotor-fuselage-combinations. Calculations are made by variation of advance ratio, rotor height and fuselage aft section.

Symbols

A influence matrix of the rotor and body
a speed of sound; vortex distance
 a_1 longitudinal angle of the tip path plane
B influence matrix of the wake
 c_n normal force coefficient
 H_{RoFD} distance between rotor head and fuselage datum line
Ma mach number
 \underline{r} vector to a vortex element
R rotor radius
t, n main stream direction; cross-flow direction
 Δt time step
 U_e velocity at the outer edge of the boundary layer
U, V main stream velocity, respectively cross flow velocity

u, v velocity in x-direction, respectively in y-direction
 V_∞ onset velocity
 V_d resultant velocity normal to the tip path plane
 V_{xRo}, V_{zRo} onset velocity components in respect to the rotor plane
 V_z vertical component of onset velocity in respect to the tip path plane
 w_i induced velocity in the tip path plane
 \underline{X} wake node location
x, y, z Cartesian coordinates; coordinates of the computational mesh of the boundary layer (curvilinear)
 Δx distance of varied geometry of fuselage aft section
 α angle between main stream direction and local integration direction (x)
 α_{Ro} angle of attack between onset flow and rotor plane
 β limiting streamline angle
 Γ vortex strength
 ϕ potential
 λ resultant angle of $\alpha + \beta$
 ϕ perturbation potential
 ν kinematic viscosity
 μ advance ratio
 Ω rotor angle velocity

Subscripts

B Betz's vortex core
FD fuselage datum
i induction (rotor actuator disc)
N number of panels
n normal direction; cross flow direction; time step
P point in space
Q, S, D sources; sinks; doublets
Ro rotor
S on surface
tpp tip path plane
v viscous; respect to vortex
 $\partial/\partial n$ differentiation to the normal direction
 ∇ gradient operator
 ∞ infinity

1. Introduction

The treatment of interactional aerodynamics of helicopter configurations can be divided into several problem zones. First, there are the rotor blades responsible for lifting and pushing the rotorcraft. The rotating blades initiate the streaming air to relative high unsteadiness onto the blades themselves. They lead to much greater complication describing the dynamical behaviour and vibration, respectively noise. Naturally, a fuselage is needed, containing all other components to be used. The fuselage shape is more or less streamlined.

In the past aerodynamicists have concentrated their labour on the first problem - increasing rotor performances under considerations of tolerable noise and vibration. In the mean time one's attention is directed to better design of fuselage shapes, aiming at reduced parasite drag of the airframe.

Both stages in improvement of rotorcraft aerodynamics are done without consideration of interactional aerodynamics and their interferences with each other. It was suggested that research efforts were furthered by the development of US Army utility transport and attack helicopters with requirements of very compact design and therefore very close fitting of rotor - airframe /1/. Following this pioneering work, many other researchers (as Wilson, Freeman, Sheridan, Betzina, Clark and Maskew, respectively Polz) gave the interaction problem serious consideration. Extensive experimental and analytical efforts were funded by NASA, some in the european domain. Till today these have achieved much success but with only moderate accuracy.

In addition to the blade to blade interferences unsteady fuselage airloads become serious. The time dependence results mainly from periodic penetration of the shed rotor blade tip vortices of the advancing front rotor section and results only marginally from the shed vortex layer of the blade trailing edge onto the fuselage shape. Several new codes were developed at the Georgia Institute of Technology and Analytical Methods Incorporation. These codes have the advantage that the interaction of rotor/body with global interaction of rotor, fuselage and rotor wake, respectively "free wake", can be calculated. Local viscous effects on the fuselage potential flow are described by Bliss' model /11 / but effects on the development

of the fuselage boundary layer are not yet known. Turbulence models with much higher influence of entrainment through the boundary layer edge must be developed to describe the real close fuselage flow under penetration of strong vortices, such as rotor blade tip vortices /14/. This may be the subject of future research.

Nevertheless it could be helpful, to get derivatives and coefficients for computing performances and simulating flight maneuvers, respectively stability under better consideration of rotor interferences on fuselage loads. Particularly in the flight regime of moderate to high speed forward flight forces and moments acting on fuselage take on an important role. Although the fuselage flow becomes complicated with disturbing rotor flow in the vicinity of the body, numerical methods treating this should be simple to handle and require moderate computer times.

Not only the upper front fuselage body is influenced by rotor and rotorwake, where the wake seems to penetrate the fuselage shape, but also the whole fuselage flow is changed due to the rotor disturbance. Therefore it is assumed, that boundary layer separation of the fuselage flow is also changed and leads to important additional fuselage airloads and subsequent changed trim state.

The following method is based upon the old fashioned principle of dividing the flow round the helicopter into two regimes: iterative coupling of the local fuselage shear layer with the global inviscid vorticity containing outer flow. The refinement of fuselage shape does not seem to be restricted (1000 or more panel allowed).

With the aid of the computed results it is aimed at gaining some insight into the fuselage flow behaviour and location of the separation line at the rear part of the fuselage. Parametric investigations were made into the influence of rotor height, advance ratio and fuselage aft section.

		fuselage A	fuselage B	fuselage C
H_{R0FD}	1,37 m	$\mu = 0,115$	0,115	0,115
	1,17 m	0,183	0,183	0,183
	0,97 m	0,32	0,32	0,32

Table 1: Parameter variation for rotor/body interference study

Values are shown in Table 1. For all configurations only some important results are listed and discussed.

2. Brief Description of the Theoretical Methods

In detail there are three major computational components involved in the program. First a conventional trim algorithm gives the flight state followed by the inviscid flow computation enclosed rotor wake and boundary layer computation coupled together.

2.1. Trim Algorithm

First, it must be stated that a fully coupled computational technique requires including the trim state computation and the downwash of the rotor within the whole solution of interferences, rotor to fuselage and reverse. Thus calculations were made to evaluate the influence of the fuselage on power required and rotor blade flap angles considering the straight interaction of fuselage on the rotor. Results were obtained from the performance calculation, which indicates no significant change in power required, some graduate flap angles and also marginable phase shifting of blade flapping. In this case it was assumed, that the calculation of the trim state needs no feed back of fuselage interference to the rotor when the task requires concentrated labour on the interaction of the rotor on fuselage. Figure 1 shows the flow velocities at the rotor disc, for example at forward flight descent. Induced velocities are defined in the tip path plane.

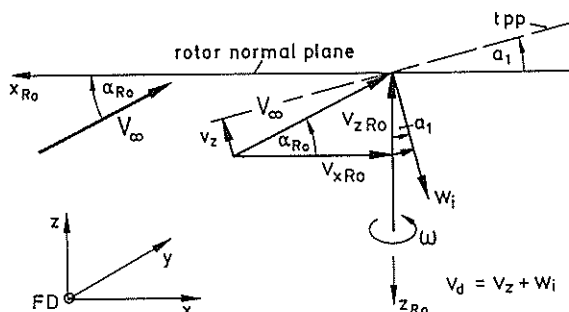


Figure 1: Velocity scheme in forward flight descent

2.2 Representation of Rotor Flow and Wake with Panel Methods

Panel methods use the relations of velocity or acceleration potential to solve continuity and momentum in any fluid flow problem. The acceleration potential method provides a simple method of describing a pressure jump. For subsonic, and like incompressible, adiabatic flows the full potential equation is reducible to the linearized so called Laplace's Equation. This equation solves Bernoulli's Equation and continuity identically in space.

$$\begin{aligned} &\Phi_{xx} \left(1 - \left(\frac{\Phi_x}{a}\right)^2\right) + \Phi_{yy} \left(1 - \left(\frac{\Phi_y}{a}\right)^2\right) + \Phi_{zz} \left(1 - \left(\frac{\Phi_z}{a}\right)^2\right) \\ &- 2 \frac{\Phi_x \Phi_y}{a^2} \Phi_{xy} - 2 \frac{\Phi_x \Phi_z}{a^2} \Phi_{xz} - 2 \frac{\Phi_y \Phi_z}{a^2} \Phi_{yz} = 0 \end{aligned} \quad (2.1.1)$$

$$\begin{aligned} \Phi_{xx} + \Phi_{yy} + \Phi_{zz} = 0 \quad &\text{for } a \rightarrow \infty \\ &\text{Laplace's equation} \end{aligned} \quad (2.1.2)$$

The linearization yields the advantage of superposing all potentials to be considered. So it is used to form the potential divided in onset flow and perturbation potential. The gradients of potential give the velocity of the flow.

$$\begin{aligned} \Phi = \Phi_\infty + \varphi \quad &\underline{x} \rightarrow \infty: \varphi \rightarrow 0 \Rightarrow \underline{v} \rightarrow 0 \\ \nabla \Phi_\infty = \underline{v}_\infty \end{aligned} \quad (2.1.3)$$

$$\nabla \varphi = \begin{pmatrix} u \\ v \\ w \end{pmatrix} = \underline{v} \quad \frac{\partial \varphi}{\partial n} \Big|_S = -\underline{n} \cdot \underline{v}_\infty \quad (2.1.4)$$

Boundary conditions are satisfied at infinity by vanishing the perturbation potential induction, and on body surface the kinematic relationship does not allow penetration through the surface, respectively fuselage shape.

In order to investigate no further refinement one can solve Laplace's Equation with the potential of the rotor, rotorwake and the fuselage (following Green's theorem, see 2.1.5 - 2.1.7). Body thickness as well as lift is represented by distributions of sources, and sinks and doublets.

$$\phi(P) = \phi_{QS}(P) + \phi_D(P) \quad (2.1.5)$$

$$\phi_{QS}(P) = -\frac{1}{4\pi} \iint_S \frac{\sigma(S)}{r(S,P)} dS \quad (2.1.6)$$

$$\phi_D(P) = \frac{1}{4\pi} \iint_{S_i} \mu(S_i) \frac{\partial}{\partial n} \left(\frac{1}{r(S_i,P)} \right) dS_i \quad (2.1.7)$$

With the discretisation of fuselage shape and rotor (divided into actuator disc panels, see Figure 2) one obtains a linear, algebraic equation system to be solved in the boundary regime with the known boundary conditions.

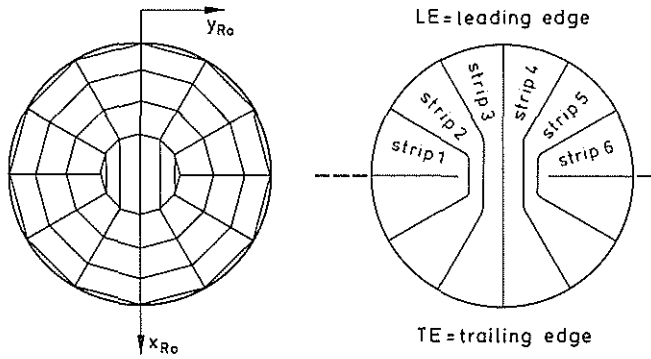


Figure 2: Bended strips representing lifting surfaces

The well known conditions in the rotor disc, or rather in the tip path plane (tpp) of the rotor evaluated earlier in the trim program stage, bring out the induced velocities in the tpp. They are to be shifted to the right hand side of equation 2.1.9. The influence on the separating wake of the rotor disc is also known in time step n and therefore also to be shifted to the right hand side of equation 2.1.9.

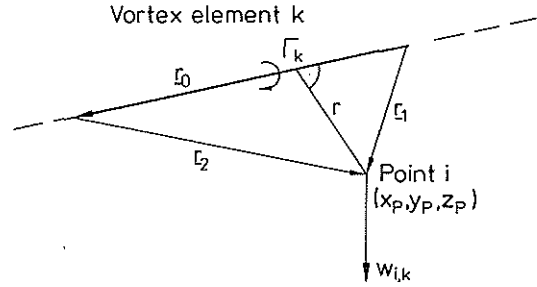
$$\sum_{j=1}^N A_{ij} \Gamma_j + \sum_{k=1}^l B_{ik} \Gamma_k' = w_i \quad (2.1.8)$$

$$\sum_{j=1}^N A_{ij} \Gamma_j = w_i - \sum_{k=1}^l B_{ik} \Gamma_k' \quad (2.1.9)$$

The new wake node locations are evaluated with simple adding of all influences, rotor and fuselage and wake together.

$$\underline{X}_i^{n+1} = \underline{X}_i^n + (\underline{V}_{i\infty} + \underline{v}_i^n) \Delta t$$

In this numerical approach several difficulties arise within the treatment of Biot Savart's Law on vortex elements, see Figure 3.



$$-w_{i,k} = \frac{\Gamma_k}{4\pi} \frac{r_0}{|l_1 \times l_2|} \left(\frac{l_0 \cdot l_1}{r_0 r_1} - \frac{l_0 \cdot l_2}{r_0 r_2} \right) \Gamma_k$$

Figure 3: Biot Savart's law of a straight vortex element

Nodes i, close to the inducing vortex element, should be damped as occurs in nature for a viscous vortex core, here the Bliss' core model is used (2.1.10). Other authors use modifications in the grid location and define secondary distributed vortex elements to avoid these problems. In this approach it was not necessary. Further on there is an aging of the vortex elements of the wake due to time implemented, this was taken into account with Oseen's formula (2.1.11) /12/.

$$\Gamma(r) = \begin{cases} \Gamma \left(\frac{r}{a_v} \right)^2 \left(2 \frac{a_v}{a_B} - \left(\frac{a_v}{a_B} \right)^2 \right)^{\frac{1}{2}} & 0 \leq r \leq a_v \\ \Gamma \left(2 \frac{r}{a_B} - \left(\frac{r}{a_B} \right)^2 \right)^{\frac{1}{2}} & a_v \leq r \leq a_B \\ \Gamma & r \geq a_B \end{cases} \quad (2.1.10)$$

$$V_\theta = \frac{\Gamma}{2\pi r} \left(1 - \exp \left(-\frac{r^2}{4\nu t} \right) \right), \quad V_r = 0 \quad (2.1.11)$$

The fuselage is represented by hundreds of quadrilateral panels each with constant strength of source or sink following Hess' pioneering work in the sixties. Together with the stepwise growing rotor wake sheath the strength of singularities of the fuselage panels will be distributed. Summing up all influences leads to the velocity and pressure distribution on the fuselage shape and brings the input data to the boundary layer computation. Other algorithms for distinguished treatment of the far field and near field influence computation, as for example clustering /10/, are not implemented.

2.3 Boundary Layer Computation

The two most important treatments of boundary layer computations in the 3-D regime are the difference method and the integral method. Both methods are derived from earlier 2-D treatments. In this approach the integral method for arbitrary three-dimensional turbulent compressible adiabatic boundary layer was chosen /13 /. The integral method uses the advantage of parametric laws to describe the boundary layer flow profile (Coles profiles); 2-parametric in the mainstream direction and 1-parametric in crossflow direction (Mager and Johnston profiles).

The main advantages against difference methods are simple handling and only 1-parameter input, for example potential velocity distribution thus rendering it easy for coupling with potential method. In order to guarantee the treatment of arbitrary shaped bodies in flows with various but moderate angles of attack, non-orthogonal curvilinear coordinates are used, see Figure 4 and 5.

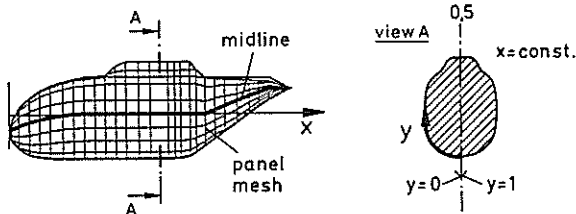


Figure 4: Coordinates on fuselage for boundary layer computations (global → curvilinear)

The body shape is expanded to the physical plane of x, y- coordinates. The three-dimensional velocity profile has to be related to the physical coordinates, see equation (2.1.12).

$$u = \frac{U \sin(\lambda - \alpha) - V \cos(\lambda - \alpha)}{\sin \lambda}$$

$$u_1 = U_e \frac{\sin(\lambda - \alpha)}{\sin \lambda} \tag{2.1.12}$$

$$v = \frac{U \sin \alpha + V \cos \alpha}{\sin \lambda}$$

$$v_1 = U_e \frac{\sin \alpha}{\sin \lambda}$$

Locally, two distinct directions t and n exist for the description of the velocity profiles. The t-direction is defined by projection of main stream velocity U_e at the outer edge of the boundary layer onto the surface, n means that perpendicular to t, respectively crossflow direction. The angle between t and x-direction of the physical plane is α . The angle β is defined by the displacement of resultant surface shear direction and the streamwise direction t.

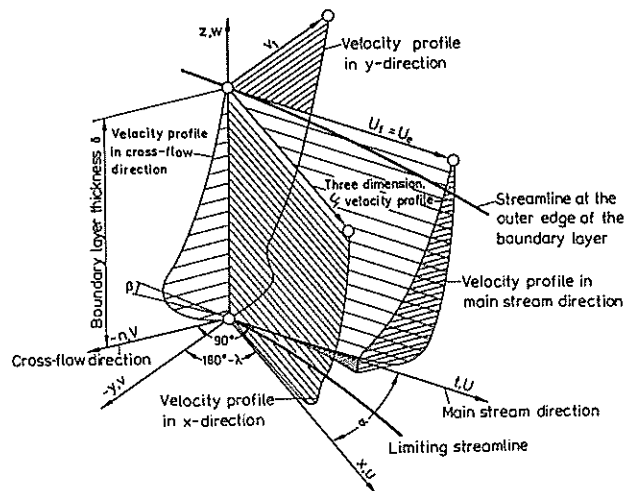


Figure 5: Schematic sketch of velocity profiles in a three-dimensional boundary layer

Several integral methods of 3-D boundary layer computations have been developed in recent years and improvements to earlier codes were made, such as the treatment of laminar and turbulent boundary layers together in the same code. The following basic equations are to be used to describe the boundary layer development on the fuselage surface:

equation of continuity

moment in x-and y-direction

integral of momentum

entrainment

lag entrainment .

Entrainment of inviscid outer flow material into the boundary layer is described by Horten's /17 / correlation of entrainment to the mean shear stress of the outer part of the boundary layer. History effects are taken into account with an empirical correction of the entrainment concept of the boundary layer in equilibrium. The moment of momentum relations means weighting of the moment development in the boundary layer downstream.

The output of boundary layer computation contains mainly the momentum loss, displacement and layer thicknesses but also resultant wall friction coefficient, respectively the angles of limiting streamline and shear direction. For inviscid/viscous coupling an equivalent outflow is given in the control points.

2.4 Coupling Procedure

Two different panel models, wide- and fine-meshed, were used in the determination of interferences of rotor and wake on the helicopter fuselage. The simple body shape (with about 50 panel) was derived from the fine-meshed B0 105 model (ca. 700 panel).

The flow chart of the solution procedure is shown in Figure 6. After definition of input data to the panelling and trim procedure a balanced flight state is obtained with flight state values i.e. angle of attack, side slip angle, onset velocity,

angles of tip path plane and downwash distribution in the rotor plane. The trim algorithm contains a conventional blade element model of the rotor and global considerations of the aerodynamic forces and moments of the airframe.

All data are known to compute the rotor wake in the presence of the fuselage. The wake solution is always determined with a wide-meshed fuselage panel model so as to decrease consuming computer time.

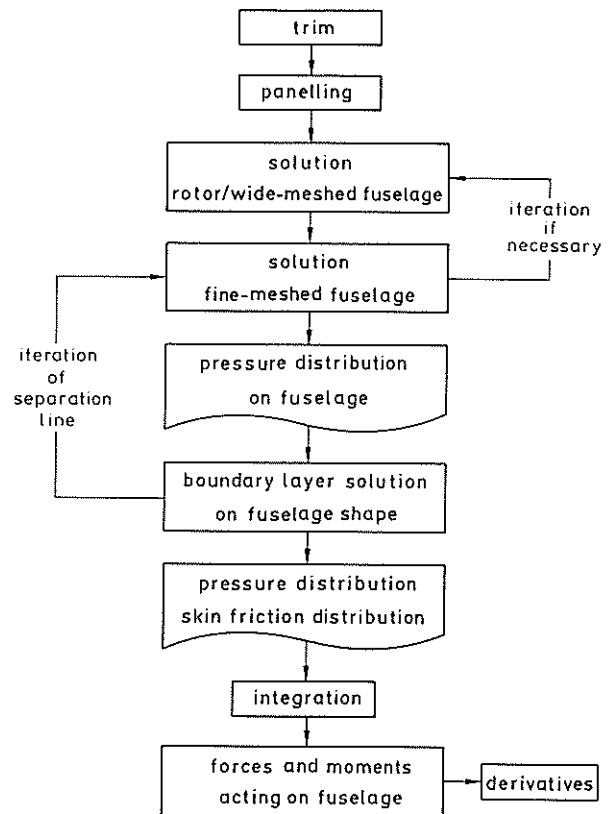


Figure 6: Flow chart of the solution procedure deriving forces and moments acting on fuselage

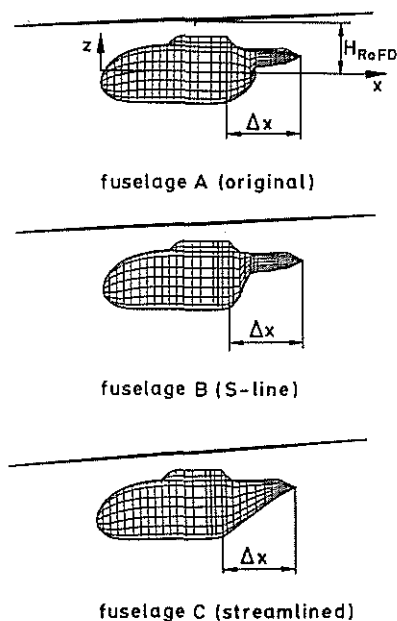
If any discrepancies occur in the offbody-velocity distribution (rotor actuator disc) due to fine-meshed panel model, an iteration loop is started to converge the velocity distribution.

This procedure consumes only moderate computer time because the time stepping wake shedding procedure is dominant while preciseness of pressure distribution on the fuselage shape is not downgraded. It is obvious, that a thousand or more

panels in the fuselage model may be used. The improvement of this concept means a higher order method in the computation of fuselage flow and pressure distribution with the interactional influence of rotor downwash and wake on it. The number of iteration cycles between the two solutions is usually 2 or 3.

3. Model Geometry

Table 1 on previous page contains the variation of all parameters. The fuselage shape is varied twice in the aft section, giving three different fuselage shapes, see Figure 7.



Shape modification in section Δx

Figure 7: Three different fuselage shapes originated from Bo 105 fuselage panel model

The original BO 105 fuselage panel model contains about 600 quadrangular panels. The first aft section variation is built up of a bottom line which matches the cylindrical body to the tailboom in smooth curvature like S-line. The circumferential panel nodes are placed equidistant. The second variation has linear stretched aft section, see Figure 7.

How the wake model works is shown in Figure 8. The above picture has no fuselage body for clearness. Since a very crude rotor model is used, all characteristic features of rotor flow with free wake is carried out.

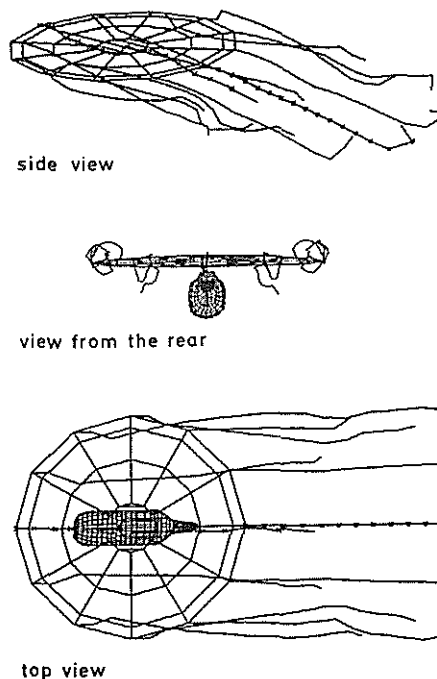


Figure 8: Different views of rotor wake formation at $\mu = 0.115$

Figure 9 gives the rotor wakes at various advance ratios, fuselage shapes and rotor heights. The rotor height is varied in 3 stages : normal, 20 cm below normal and 40 cm below normal. The advance

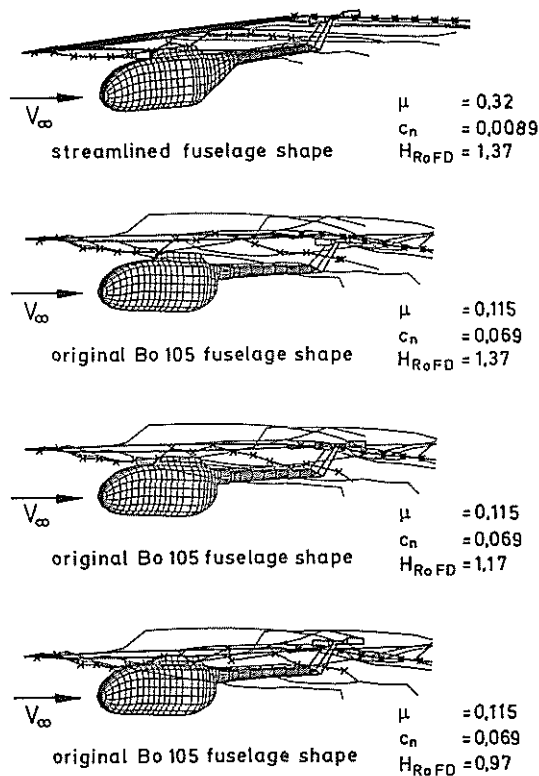


Figure 9: Rotor flow at various advance ratios, fuselage shapes and rotor heights

ratio is related to the freestream velocity with no rotor incidence, so the advance ratio are derived from $V = 25 \text{ m/s}$, 40 m/s and 70 m/s . The indicated normal force coefficient is related to the freestream velocity and always gross weight of 2000 kg. Figure 9 makes clear the different trim situation of advance ratio 0.32 against 0.115 with quite different angle of attack. But also the brave shedded wake from the rotor disc as cited above is in good correlation with large scale models. The front and rear wake line is noted with cross and starpoints and thereby tracing the developing wake in the presence of the fuselage body. The front line seems to be pushed strong enough by the body as it crosses the rotor disc up and down.

4. Theoretical Results and Comparison with Experimental Data

4.1 Trim Solution and Flight State

Always non accelerated flights were taken as entrance for these studies. The gross weight was fixed at 2000 kg. The computations of pressure distributions were made with a range of $\pm 30^\circ$ in angle of attack and $\pm 10^\circ$ in side slip. The boundary layer studies are based upon the 3 different velocities as mentioned earlier in Table 1.

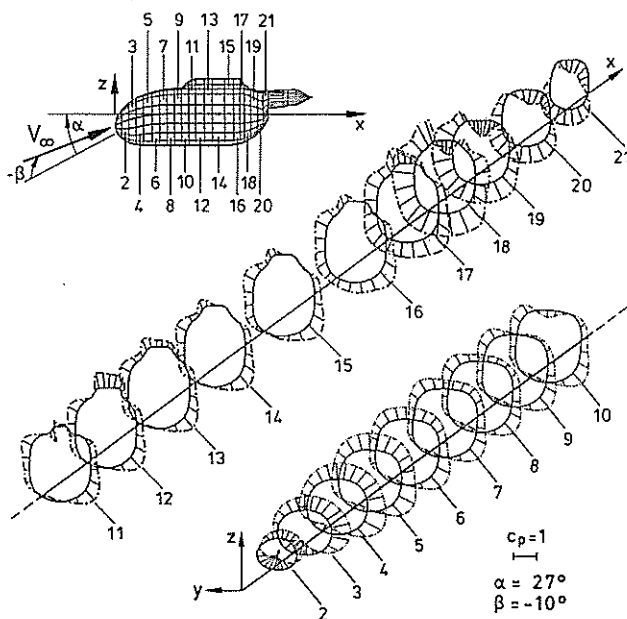


Figure 10: Pressure distribution on Bo 105 fuselage shape at $x=\text{const.}$ stations in forward flight descent and slip

4.2 Fuselage Pressure Distribution

About 600 source panels were used in the potential flow model for representation of the original Bo 105 fuselage. Pressure distributions have been plotted circumferentially at $x = \text{constant}$ stations (Figure 10) and versus axial distance along top

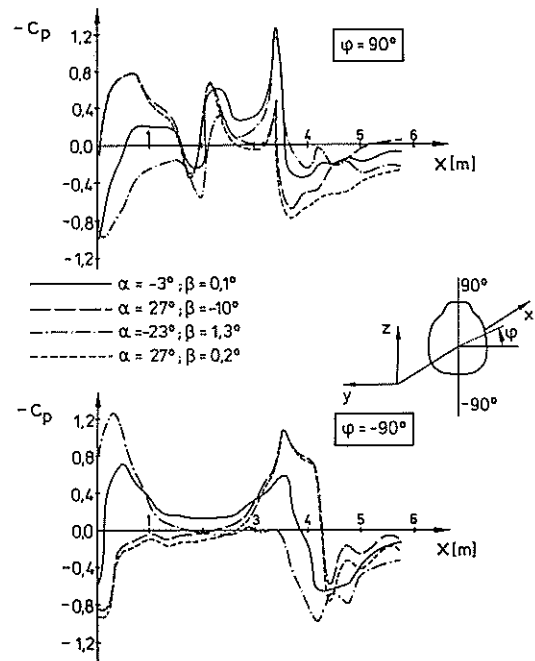


Figure 11: Pressure distribution on Bo 105 fuselage shape at constant radial stations in forward flight, (upper and lower side)

and bottom centerlines (Figure 11) and along power unit fairing and waterline (Figure 12). The plots shown in Figure 10 were made at steep forward flight descent with side slip. The outward directed c_p -values are negative. Two regions of accelerated flow, nose area and the fuselage aft section, with larger negative c_p -values. While in the front almost no positive pressure coefficient exists, larger areas of positive c_p -values behind power unit fairing are shown. The area of most interest is located in the change of the cylindrical to the aft section with high flow acceleration and deceleration.

The pressure distributions plotted in Figure 11 were made at various flight states. Horizontal flight with climb and descent and also side slip were considered. The high pressure gradients as mentioned in Figure 10 are shown clearly. Horizontal

tal and climbing flight generate these pressure gradients on top of the fuselage shape, while at descent flight higher positive c_p -values on the bottom occur.

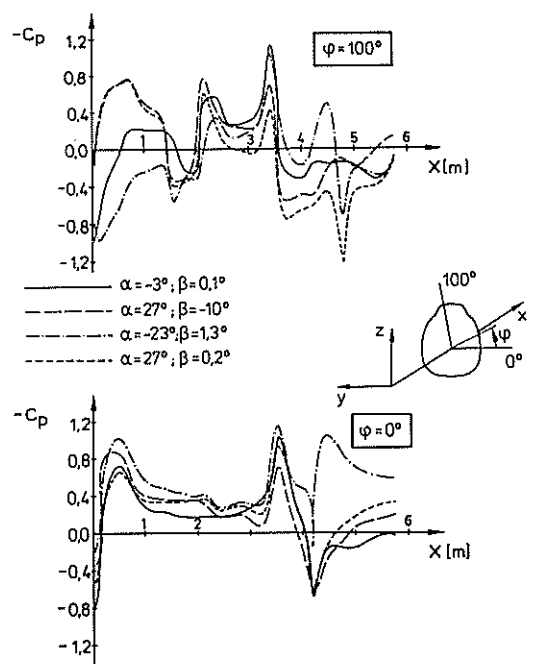


Figure 12: Pressure distribution on Bo 105 fuselage shape at constant radial stations in forward flight, (port side and close to fairing of power unit)

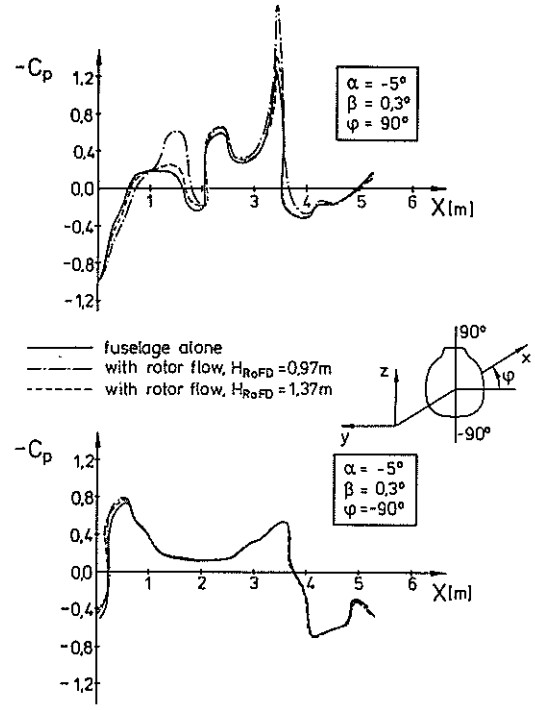


Figure 13: Pressure distribution on Bo 105 fuselage shape at constant radial stations in forward flight with and without rotor flow

Figure 12 shows the pressure distributions right beside the power unit fairing and along the waterline. The top hand diagram is comparable to those in Figure 11. Thus the waterline pressure distribution is naturally less affected by flow angle of attack. The same behaviour as mentioned in Figure 11 is identified in the aft section area, because the contraction of the fuselage body is semispherical formed.

The influence of rotor downwash and wake is shown in Figure 13, for a fast horizontal flight, respectively high advance ratio. The results are compared to the unaffected fuselage. The influence of rotor height is considered by two different rotor/body clearances. There are some effects in the forward and rearward area of power unit, with higher c_p -values in the case of lower rotor/body clearance.

4.3 Boundary Layer Analyses

The different pressure relations of Figures 10-13 cause various kinds of boundary layer developments on the fuselage shape. The next figure shows the particle tracing of the potential flow projected onto wall, respectively body shape, and the angle between the resultant skin friction direction and the flow direction x. This points out at least the rotor and wake influence in a qualitative manner.

Beginning with the original BO 105 fuselage, the rotor influence is studied at low advance ratio and original rotor clearance, shown in Figure 14. While the fuselage flow alone shows symmetry, the rotor influence causes slight unsymmetry, particular in the windward aft section. Further on the particle tracing lines are shifted versus bottom line when the rotor is considered. The cross flow angles seem to remain moderate, but become weaker when the rotor is on. Very large divergence is shown in the aft section, but normally the boundary layer is separated. Several numerical problems exist for plotting the cross flow angle tracing.

Care should be taken into account when regarding the results of boundary layer computation, because the 3-D fuselage shape is transformed the 2-D computational mesh and therefore distortion of the front and rear part occurs.

The features described in Figure 14 are also shown in Figure 15 with the streamlined fuselage shape. The rotor penetrates the fuselage flow slightly downward to bottom line with greater effects in the aft section area. This means unfortunately separation going upstream in the bottom area of the aft section.

In contrast to Figure 14 and 15, a higher advance ratio is considered in Figure 16. Rotor clearance is normal. Because of the very slight rotor induction and therefore weak rotorwake the influence within the fuselage flow is less than for lower advance ratios or higher rotor disc loadings. Some boundary layer developments in this case appear quite "favourable". Subsequently, the influence of rotor/body clearance is studied, shown in Figure 17. The bottom remains less affected but at the top area an influence is identified. Unsymmetrical flow such as side slip occurs and the cross flow angle become larger. The streamlines in the upper front area diverge slightly more due to the rotor influence when rotor/body clearance become lower.

In addition to the particle tracing plot an iso-contour plot of the momentum loss thickness is shown in Figure 18, with the same conditions as described in Figure 15. The rotor influence changes the distribution of momentum loss thickness definitely. Their boundary layer development in the area of power unit and the "windward" side seems to be stronger than without rotor flow. The separation line at the bottom seems to be shifted upstream. This was also indicated by diverging of the streamlines, shown in Figure 15.

Another remarkable relationship of separating boundary layers is the skin friction development downstream. In Figure 19 the iso-colour picture of the skin friction coefficient show the influence of rotor height. The fuselage surface is divided into regions of non-separated and separated boundary layer. The front part indicates no differences due to rotor/body clearance, meaning that the same skin friction on the fuselage surface is evident. In the mid section separation occurs on the surface of the power unit fairing, indicated by large negative skin friction gradients. The integral approach used in the present method has no ability for relaxing turbulent separated flow, but the computation is continued, although some boundary layer values violate the

integral relationships after separation. Therefore one should not have complete confidence in the treatment of this part of the fuselage flow. The values in the rear part, whole aft fuselage section, indicate boundary layer separation independent of rotor/body clearance.

The computations were made with variation of all involved parameters, only a few results are chosen for the indication of rotor fuselage interference. The shown separation lines in Figure 20 were computed with the present method and then compared to Gillespies' experimental results, respectively MBB's computational results. The former installed shape factor, consisting of the quotient of momentum loss thickness with boundary layer thickness, successful in the quasi - 2-D regime of infinite swept wings, was not used as a separation indicator but instead of this the momentum loss thickness was used alone. The values of skin friction coefficient were decided to be less favourable in this task.

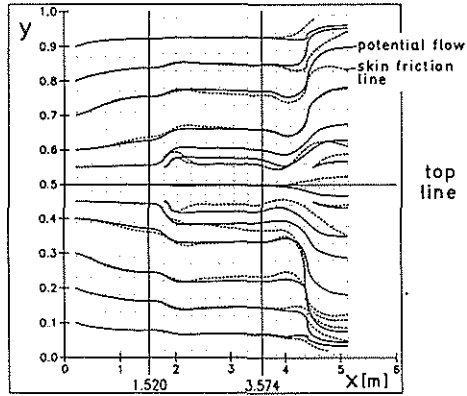
Figure 20 show the compared results of the above mentioned cases, the foreign data are originated from Boeing Vertol and Messerschmidt Bölkow Blohm, both created in the seventies. The present results without rotor influence show noteworthy agreement with /16/. However the results from MBB are based upon the potential flow computation with a larger negative angle of attack(- 10°). Consideration of rotor influence gives slightly extended areas of separated boundary layer.

The picture below contains the rotor influence on the flow passing the streamlined fuselage shape. Funded description of the flow behaviour on the side part of the aft section is not feasible in this approach. However the separation line at the fuselage bottom going upstream due to rotor influence is plausible. But a definite prescription of resultant fuselage drag seems to be yet impossible or at least difficult.

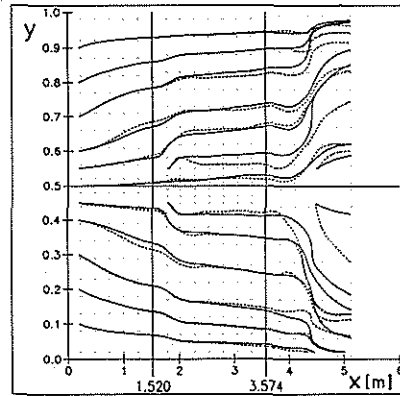
fuselage A
(alone)

Ma = 0,073 ; $\mu = 0,115$
 $\alpha = 1,5^\circ$
 $\beta = 0^\circ$
 $c_n = 0,069$

fuselage A
(rotor on)
 $H_{RoFD} = 1,37m$
(normal clearance)



rotor flow and wake not considered

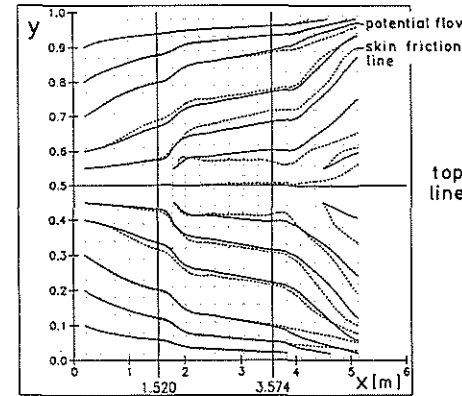


influence of rotor wake

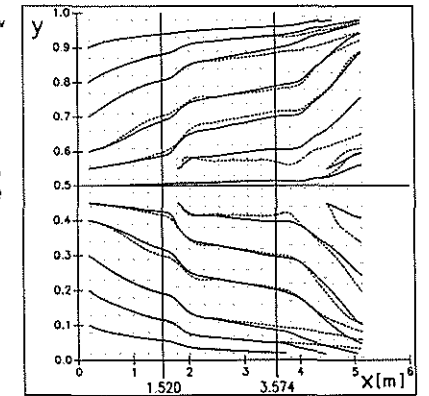
fuselage C
(alone)

Ma = 0,206 ; $\mu = 0,32$
 $\alpha = -5^\circ$
 $\beta = 0,3^\circ$
 $c_n = 0,0089$

fuselage C
(rotor on)
 $H_{RoFD} = 1,37m$
(normal clearance)



rotor flow and wake not considered



influence of rotor wake

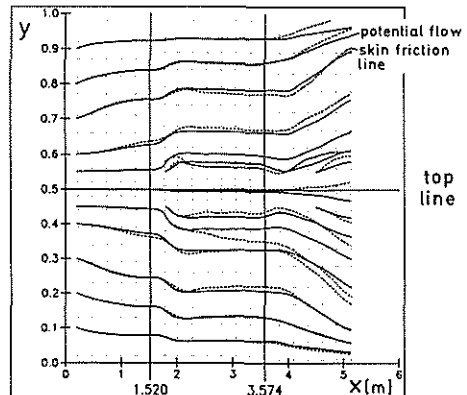
Figure 14: Particle tracing on original fuselage at $\mu=0.115$

Figure 16: Particle tracing on streamlined fuselage at $\mu=0.32$

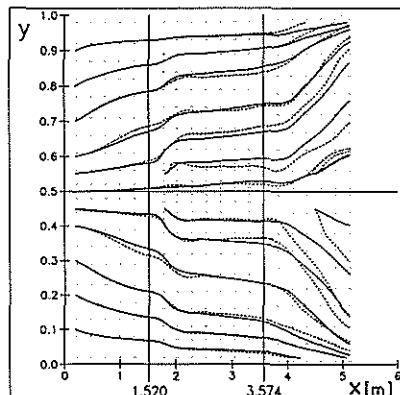
fuselage C
(alone)

Ma = 0,073 ; $\mu = 0,115$
 $\alpha = 1,5^\circ$
 $\beta = 0^\circ$
 $c_n = 0,069$

fuselage C
(rotor on)
 $H_{RoFD} = 1,37m$
(normal clearance)



rotor flow and wake not considered

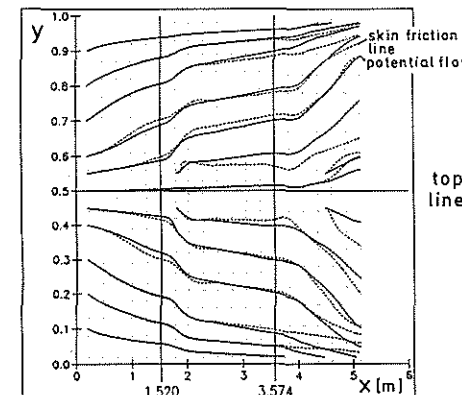


influence of rotor wake

fuselage C
(rotor on)
 $H_{RoFD} = 1,37m$
(normal clearance)

Ma = 0,206 ; $\mu = 0,32$
 $\alpha = -5^\circ$
 $\beta = 0,3^\circ$
 $c_n = 0,0089$

fuselage C
(rotor on)
 $H_{RoFD} = 0,97m$
(low clearance)



influence of rotor height

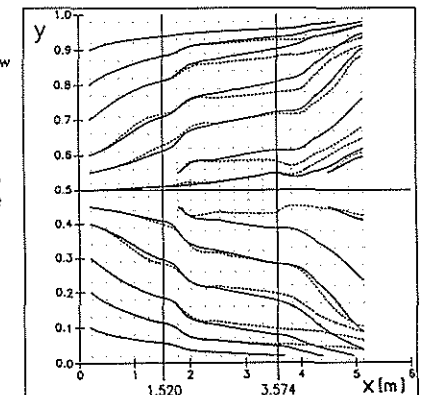


Figure 15: Particle tracing on streamlined fuselage at $\mu=0.115$

Figure 17: Particle tracing on streamlined fuselage at $\mu=0.32$

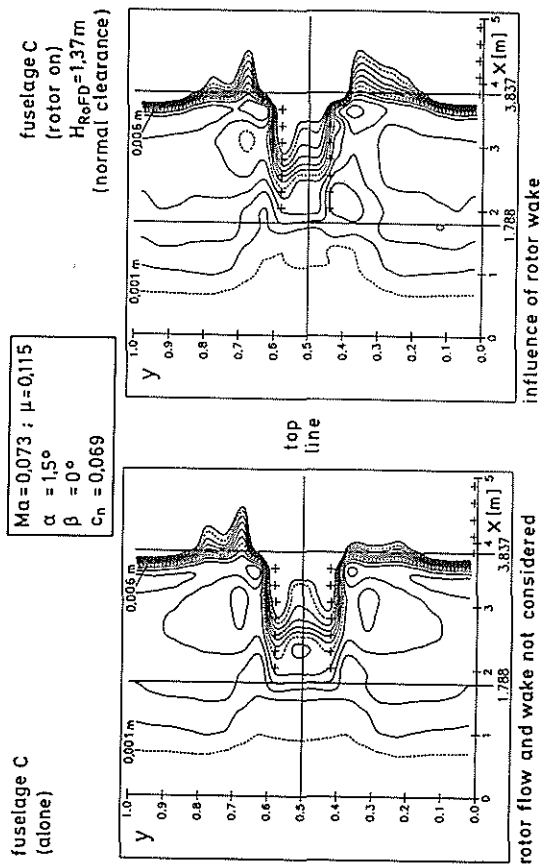


Figure 18: Iso contour-lines of momentum loss thickness

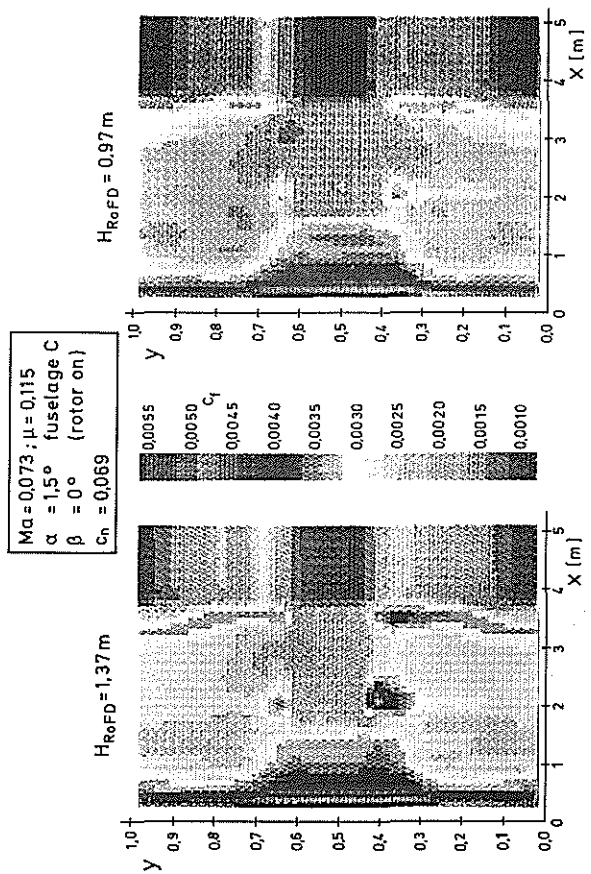


Figure 19: Skin friction on streamlined fuselage at $\mu = 0,115$

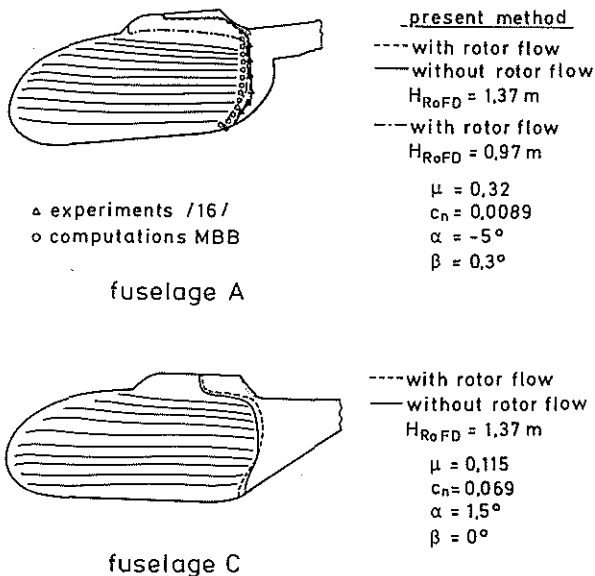


Figure 20: Separation lines on different fuselage shapes, various conditions of onset flow

5. Some Aspects of the Windtunnel Model

The present situation is a fairly large but inconsistent amount of experimental data available in the literature. The data should be for the fuselage alone and rotor-fuselage configuration. Identical test conditions for the same model should be required for the following data:

- aerodynamic forces (and moments) on rotor
- aerodynamic forces and moments on fuselage
- pressure distribution on fuselage shape
- inflow velocity distribution just above rotor plane
- offbody velocity near the empennage
- flow visualization on fuselage shape

The variation of some geometry parameters such as rotor/fuselage clearance and fuselage body shapes within altered rotor loading and flight state including side slips will complete an overall data base for validation of codes.

In the mean time a 1:6.75 scaled model, see Figure 21 with diameter 1.5 m is developed at the Institute of Flightmechanics at the Techn. University of Braunschweig and will be installed in the 3 m x 3 m test section of the DLR windtunnel in Braunschweig. After a test period there are planned measurements to obtain experimental data and to validate the theoretical results and give more detailed data base.

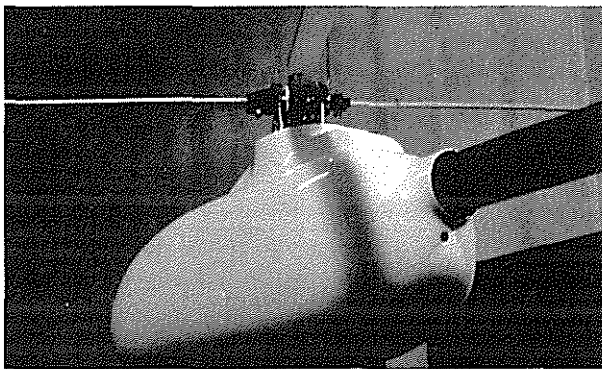


Figure 21: Modular windtunnel model of the Bo 105 helicopter

6. Conclusion

The treatment of interactional aerodynamics in the design prephase of a new helicopter generation will become more serious in the future. Some problems will be studied in the averaged time domain. A method in this manner has been developed to study the influence of interactional aerodynamics, respectively rotor/body interferences, on the fuselage flow of an helicopter. Four main program devices are coupled together with iterative procedures. A conventional trim algorithm gives the entire state values. The potential flow is computed with ordinary panel methods; rotor wake is computed in the presence of the fuselage body with the free wake model. The boundary layer is computed with an integral boundary layer method. Parameters namely rotor height, fuselage aft section and advance ratio were varied. Following

summary of the achieved results:

- Rotor/body interference take on a minor role on fuselage flow with higher advance ratios due to less induced velocities of the rotor.
- The flow of the fuselage bottom is less influenced in general but the separation line is modified and therefore pressure drag will increase due to rotor downwash and wake influence.
- The rotor downwash and wake also cause slight unsymmetry of the potential flow and boundary layer development with unsymmetrical separation line. Values of side force and azimuthal moment will increase.
- The influence of rotor downwash and wake will become serious in the aerodynamical problem zones of the fuselage shape.

7. References

- /1/ Landgrebe, A.J.; Moffit, R.C.; Clark, D.R.: Aerodynamic Technology for Advanced Rotorcraft, Paper Presented at the AHS Symposium, Essington, PA, 1976
- /2/ Sheridan, P.F.; Smith, R.P.: Interactional Aerodynamics - A New Challenge to Helicopter Technology, Presented at the 35th Annual Forum of the AHS, 1979
- /3/ Freeman, C.E.; Wilson, J.C.: Rotor-Body Interference (ROBIN) Analysis and Test, Paper Presented at the 36th Annual National Forum, AHS, Washington, D.C., May 1980
- /4/ Huber, H.; Polz, G.: Studies of Blade to Blade and Rotor-Fuselage-Tail Interferences, AGARD Fluid Dynamics Panel Specialists' Meeting on Prediction of Aerodynamic Loads on Rotorcraft, London, May 1982
- /5/ Betzina, M.D.; Smith, C.A.; Shinoda, P.: Rotor/Body Aerodynamic Interactions, 9. European Powered Lift and Rotorcraft Forum, Paper 5, Sep. 1983
- /6/ Maskew, B.; Clark, D.R.: Study for Prediction of Rotor/Wake/Fuselage Interference, Part I: Technical Report, NASA Contractor Report 177340, March 1985

- /7/ Hess, J.L.; Smith, A.M.O.: Calculation of Potential Flow about Arbitrary Bodies, New York: Pergamon Press, 1966
- /8/ Maskew, B.: Subvortex Technique for the Close Approach to a Discretized Vortex Sheet, Journal of Aircraft, Vol. 14, No. 2, Februar 1977
- /9/ Hoejmakers, H.W.M.: Computational Vortex Flow Aerodynamics, AGARD Conference Proceedings No. 342: Aerodynamics of Vortical Type Flows in Three Dimensions, Rotterdam, April 1983
- /10/ Nowak, Z.P.: Panel Clustering Technique for Lifting Potential Flows in the Three Space Dimensions, In: Notes on Numerical Fluid Mechanics, Vol. 21, Braunschweig: Vieweg, 1988
- /11/ Bliss, D.B.; Teske, M.E.; Quackenbush, T.R.: A New Methodology for Free Wake Analysis Using Curved Vortex Elements, NASA Contractor Report 3958, 1987
- /12/ Kirde, K.: Untersuchungen über die zeitliche Weiterentwicklung eines Wirbels mit vorgegebener Anfangsverteilung
Ingenieur Archiv, 31. Band, 6. Heft, 1962
- /13/ Stock, H.W.: Integralverfahren zur Berechnung dreidimensionaler laminarer und turbulenter Grenzschichten
Dornier GmbH, Rep.-Nr. 77/51 B, October 1977
- /14/ Berg, B.van den; Humphreys, D.A.; Krause, E.; Lindhout, J.P.F.: Three-Dimensional Turbulent Boundary Layers-Calculations and Experiments, In: Notes on Numerical Fluid Mechanics, Vol. 19, Braunschweig: Vieweg, 1988
- /15/ Meyer, F.-W.: Ein Verfahren zur Berechnung der Rotor-Rumpf-Interferenz beim Hubschrauber, DGLR-Jahrbuch 1988, Vol.II, Darmstadt, Sep. 1988
- /16/ Gillespie, J.Jr.; Windsor, R.I.: An Experimental and Analytical Investigation of the Potential Flow Field, Boundary Layer, and Drag of Various Helicopter Fuselage Configurations, USAAMRDL TN 13, Fort Eustis, Jan. 1974
- /17/ Horton, H.P.: Entrainment in Equilibrium and Non-Equilibrium Turbulent Boundary Layers, Hawker Siddely Aviation Ltd., Hatfield, Rep. Nr. Research /1094/ HPH, 1969